Synergistic Upper-limb Functional Muscle Connectivity using Acoustic Mechanomyography

Carlos Sebastian Mancero C., Ravi Vaidyanathan*, and S. Farokh Atashzar*

***Abstract*— Functional connectivity is a critical concept in describing synergistic muscle synchronization for the execution of complex motor tasks. Muscle synchronization is typically derived from decomposition of intermuscular coherence (IMC) at different frequency bands through electromyography (EMG) signal analysis, which potentially limits out-of-clinic applications. In this investigation, we introduce muscle network analysis to assess the coordination and functional connectivity of muscles based on mechanomyography (MMG). We focus on a targeted group of muscles vital for activities of daily living (ADLs) in the upper-limb. Functional muscle networks are evaluated for ten able-bodied participants and three upper-limb amputees. Muscle activity was acquired from a custom-made wearable armband of MMG sensors placed over four superficial muscles around the forearm (flexor carpi radialis (FCR), brachioradialis (BR), extensor digitorum communis (EDC), and flexor carpi ulnaris (FCU)) while participants performed four different hand gestures. Muscle connectivity analysis at multiple frequency bands shows significant topographical differences across gestures for low ($<$ 5Hz) and high ($>$ 12 Hz) muscle activation frequencies as well as observable differences in coherence between amputee and non-amputee subjects. Results demonstrate MMG can be used for the analysis of functional muscle connectivity and mapping of synergistic synchronization of upper-limb muscles in complex movement tasks. The new physiological modality provides key insights into neural circuitry of motor coordination. Findings further offer the concomitant outcomes of demonstrating feasibility of MMG to map muscle coherence from a neurophysiological perspective and providing a mechanistic basis for its translation in human-robot interface.**

***Index Terms*— Biomechanics, muscle networks, coherence, functional connectivity, mechanomyography (MMG).**

This work was supported in part by the UK EPSRC CDT in Neurotechnology, UK Dementia Research Institute Care-Research Technology Centre (DRI-CRT), Imperial College Department of Mechanical Engineering and US National Science Foundation (Awards 2037878; 2031594). *Corresponding authors contributed equally to this work. Correspondence: S. Farokh Atashzar and Ravi Vaidyanathan.

C. Sebastian Mancero Castillo and Ravi Vaidyanathan are with the Department of Mechanical Engineering, Imperial College London (ICL), London SW7 2BU, UK, and the UK DRI-CRT, Imperial College London (ICL), London SW7 1AL, U.K. (e-mail: csm116@imperial.ac.uk, r.vaidyanathan@imperial.ac.uk).

Ravi Vaidyanathan is also with Serg Technologies, London E16 2DQ, U.K. (e-mail: r.vaidyanathan@sergtechnologies.com).

S. Farokh Atashzar is with the Department of Mechanical and Aerospace Engineering, New York University (NYU), New York, NY 10003 USA, also with the Department of Electrical and Computer Engineering, New York University (NYU), New York, NY 10003 USA, and also with NYU WIRELESS, New York, NY 11201 USA (e-mail: f.atashzar@nyu.edu).

I. Introduction

A. Functional Connectivity

Congruous coactivation and coordination of groups of muscles are centrally controlled by the nervous system for the execution of functional motor tasks. A theory strongly investigated in the last decade is that the central nervous system (CNS) simplifies this complex task by controlling coordinative neural functions, or synergies, as opposed to individual muscles [1]. Neurophysiological studies have shown that the musculoskeletal system and the nervous system work collectively to coordinate the activation of muscle synergies to execute complex functional motor behaviors [2]–[4]. The functional synergistic synchronization implies a common neural drive identified using intermuscular coherence (IMC) [5]. This method seeks to characterize the spectral synchronization of the common neural drives to groups of muscles. While classical analysis of synergies (e.g., those achieved by applying non-negative matrix factorization to EMG signals) represents the low-frequency basis of coordination in neuromuscular control, coherence analysis captures full-spectrum functional connectivity and synchronous control between muscle pairs, which can be summarized using metrics rooted in graph theory.

Historically, coherence analysis has been implemented to process electroencephalography (EEG) brain activity to correlate functional connectivity between different regions of the brain [6]. More recently, it has been proposed to investigate functional connectivity between brain and muscle activity (i.e., corticomuscular coherence (CMC)), through mapping of synchronization between EEG and electromyogram (EMG) recordings [7] [8] [9]. Furthermore, modulations of neural input to muscle groups in broader frequencies have been investigated using intermuscular coherence and the concept of muscle networks [5], [10]–[13]. Muscle network analysis is a novel toolset proposed to estimate functional connectivity between muscles. This is accomplished through the isolation of key characteristics of the neural drive of muscle synergies which enable the CNS to simplify functional control via synchronous muscle activation. Boonstra [10], for example, investigated lower-limb connectivity (synchronous activation) of muscles over a range of frequency bands during various postural tasks. In another study, Laine [14] isolated coherence between three-hand muscles (first dorsal interosseous, abductor pollicis brevis, and flexor digitorum superficialis) through analysis of muscle activation during two precision pinch tasks. Both of these studies found systematic task-specific

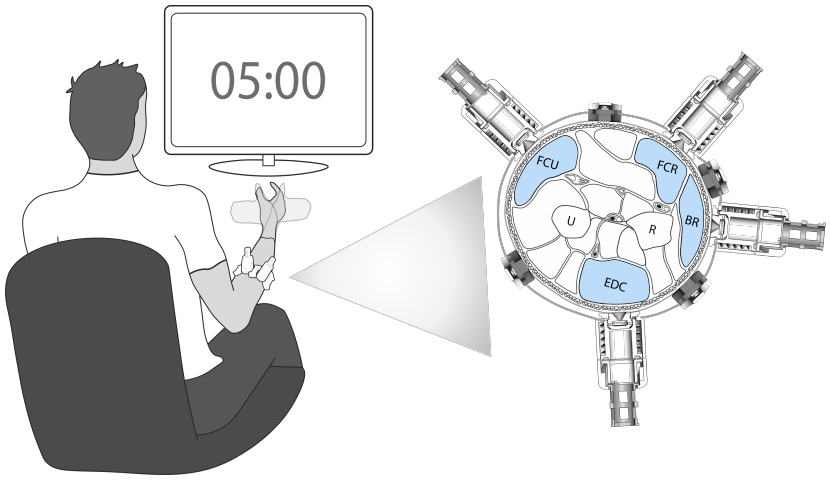

Fig. 1. Left-side, experimental layout. While seating, participants were asked to perform four hand-gesture tasks. Hand gestures were sustained for a period of five seconds with a five-second resting period between each contraction. A digital clock was presented to the participants to keep track of the duration of each contraction. Right-side, the cross-section view of MMG sensor placement. Four MMG sensors were placed over the flexor carpi radialis (FCR), brachioradialis (BR), extensor digitorum communis (EDC), and flexor carpi ulnaris (FCU) muscles.

changes and widespread connectivity of muscles at multiple frequencies bands. While conventional muscle synergy analysis seeks to identify low-frequency coactivation bases of muscles, functional muscle networks seek to group muscles based on their collective spectral response, observed as the co-modulation of multiple frequencies in EMG signals. Studies have further demonstrated conventional synergy analysis and functional coherence-based muscle network analysis elucidate disparate, complementary features of muscle activation, both of which are essential for understanding neuromuscular motor control [10] [13]. Muscle network analysis has also been studied in able-bodied individuals using EMG for hand gesture recognition [15], and in stroke survivors for the analysis of functional intermuscular connectivity alterations [16]. However, its role in compensation for neural trauma has not been extensively explored. In particular, functional connectivity variations linked to limb loss and how surgical amputation alters the behavior of muscle networks during motor tasks have not been investigated.

B. Modalities of Muscle Activity Measure

All investigations of muscle networks to date have exclusively focused on the analysis of activity through EMG. While the obvious gold standard for muscle activity mapping, EMG signal acquisition can be challenging for isolating specific muscle activation in amputees due to variations in skin impedance (e.g., sweat, scar tissue caused by surgery, etc.) and robustness of signal acquisition in sockets. Mechanomyography (MMG) is a myographic activity measure that detects mechanical oscillations produced by the dimensional changes of the active muscle fibers during a contraction [17]. MMG has been demonstrated to contain imperative information regarding neuromuscular parameters associated with motor function [18]. Investigations of this modality have revealed that spectrotemporal parameters of MMG can correlate strongly with the motor unit activation [19]. MMG has also been demonstrated to be a useful tool to assess muscle weakness characteristics and muscle performance in healthy individuals and patients [20] [21] [22]. Furthermore, MMG has been reliably described as the mechanical counterpart giving complementary information to EMG [23]. The combination of the two signals has been shown to provide unique information about the electromechanical characteristics of the muscles [24]. The benefit of MMG over EMG signal acquisition relates to the robustness to electromagnetic noises, in addition to skin sweating and sensor-skin impedance changes, as well as its response correlating to direct muscle movement [25]. However, MMG also suffers from a lack of established sensors and can demand complementary motion sensing to reject mechanical interference [26]. It should be noted that while MMG contains a lower information rate and less linear behavior when compared with EMG, in the literature, MMG has attracted a great deal of interest for practical uses where EMG may not function as well due to the electromagnetic artifacts and sensitivity to sensor-skin conditions.

C. Investigative Focus

Coherence analysis has been extensively studied through surface EMG signals to investigate the connectivity of motor neuron pools. However, the method has not been used to determine muscle connectivity by the use of MMG. In the present study, for the first time, we use MMG to assess the functional connectivity between four superficial muscles in the forearm during various hand gesture tasks. Our study is motivated by evidence in the literature demonstrating that the frequency spectrum of MMG contains critical information regarding motor unit recruitment and firing rate [27] [28], which provides a neurophysiological basis for their use in coherence analysis.

We investigate muscle network analysis during sustained hand gesture tasks in amputee and able-bodied human participants. We hypothesize that muscle networks generated from MMG signals will be task-dependent while showing synchronized behavior at multiple distinct frequency bands,

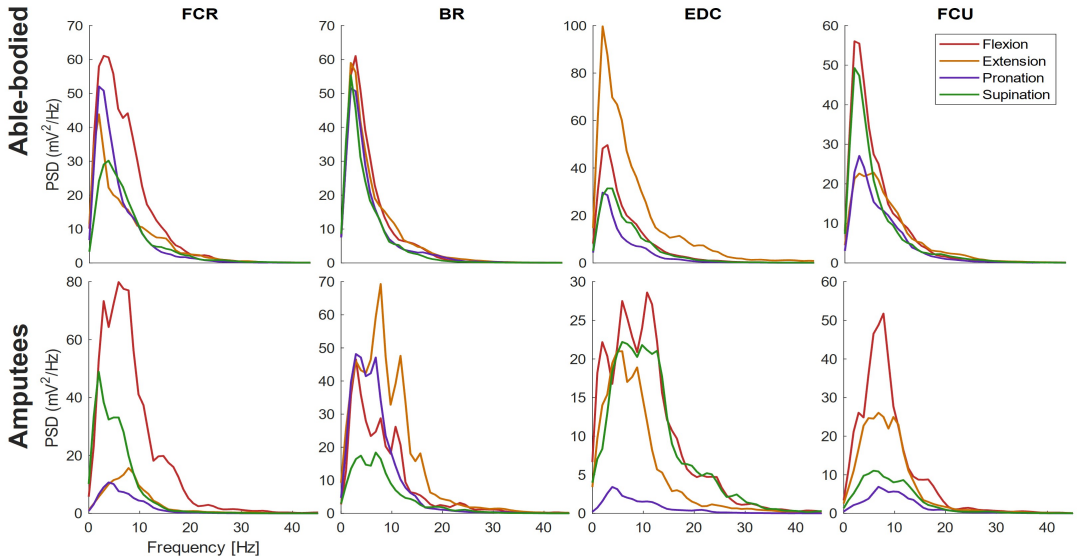

Fig. 2. Power spectral density shown for the different muscles (FCR, BR, EDC, and FCU) for all gestures (red: Flexion, yellow: Extension, purple: Pronation, and green: Supination). Power spectra were averaged across homologous muscles, trials, and subjects for able-bodied (top-row) and amputee (bottom-row) participants.

reflecting the spectral fingerprints of the motor unit pool activation. We also aim to determine muscle network characteristic differences between tasks and demographics. Furthermore, we hypothesize that functional connectivity networks derived from MMG not only show significant changes across different hand gestures but will also show identifiable variations across the two understudied demographics of amputee and able-bodied participants. Graph theoretical analysis is implemented to quantify characteristics of the network topologies and statistically compare muscle networks across four hand-gesture tasks and between the two demographics. The topology and spectral characteristics of the muscle networks provide novel insights into the neural basis of muscle synergies. Also, the characterization of MMG-based functional muscle networks can offer a new tool to examine the neural circuitry involved in motor tasks.

In summary, the main contributions of this study are:

- Identification of functional intermuscular connectivity between superficial upper-limb muscles, in various spectral bands, by the use of MMG across a cohort of amputee and able-bodied participants (ten able-bodied; three amputees)
- Identification of different muscle network topologies for each hand gesture.
- Comparison of the characteristics of muscle network patterns across both demographics.
- Identification of alterations in muscle network characteristics associated with amputation.

Beyond the first implementation of MMG in muscle network analysis, this study is the first contrasting functional comodulation of amputee and able-bodied subjects. While MMG has been studied as an alternative means of prosthetic control surmounting well-documented challenges involved in EMG use out-of-clinic [29], [30], aspects of its neurophysiological basis remain unknown.

II. Method

A. Participants

Ten able-bodied individuals (6 males, 4 females, mean age 26 $\pm$ 7 years old) and three trans-radial amputees (2 males, 1 female, mean age 38 $\pm$ 8 years old) participated in this experiment. All participants provided their signed informed consent before taking part in the study. All experiments were approved by the Imperial College Research Ethics Committee (ICREC reference: 15IC3068).

B. Experimental Design

Data collection was performed by the use of a custom-made wearable acoustic MMG armband, described in [31]. Thanks to the low effect that crosstalk has in the MMG signal in the transverse direction of propagation of the mechanical waves [32], the use of microphone-based MMG sensors, as used in the present study, results in a robust tool for the assessment of muscle activity. In addition, the level of crosstalk in the MMG signal has shown to be dependent on the level of muscle effort [33]; therefore, low level contractions of a short span (5 seconds) resembling activities of daily living (ADLs) were applied in this study. Experiments involved the detection of MMG activity while participants were asked to perform four different hand gestures, namely wrist Flexion, Extension, Pronation, and Supination. Four MMG sensors were placed around the forearm over the target muscles: flexor carpi radialis (FCR), brachioradialis (BR), extensor digitorum communis (EDC), and flexor carpi ulnaris (FCU). The participants were asked to position their dominant arm in a resting position while seated. Resting position is defined as placing the arm midway in supination at the forearm with the elbow in contact with the torso and the forearm at 90 degrees with respect to the arm. Participants were asked to stay still for the duration of the experiment. Prior to the experiment,

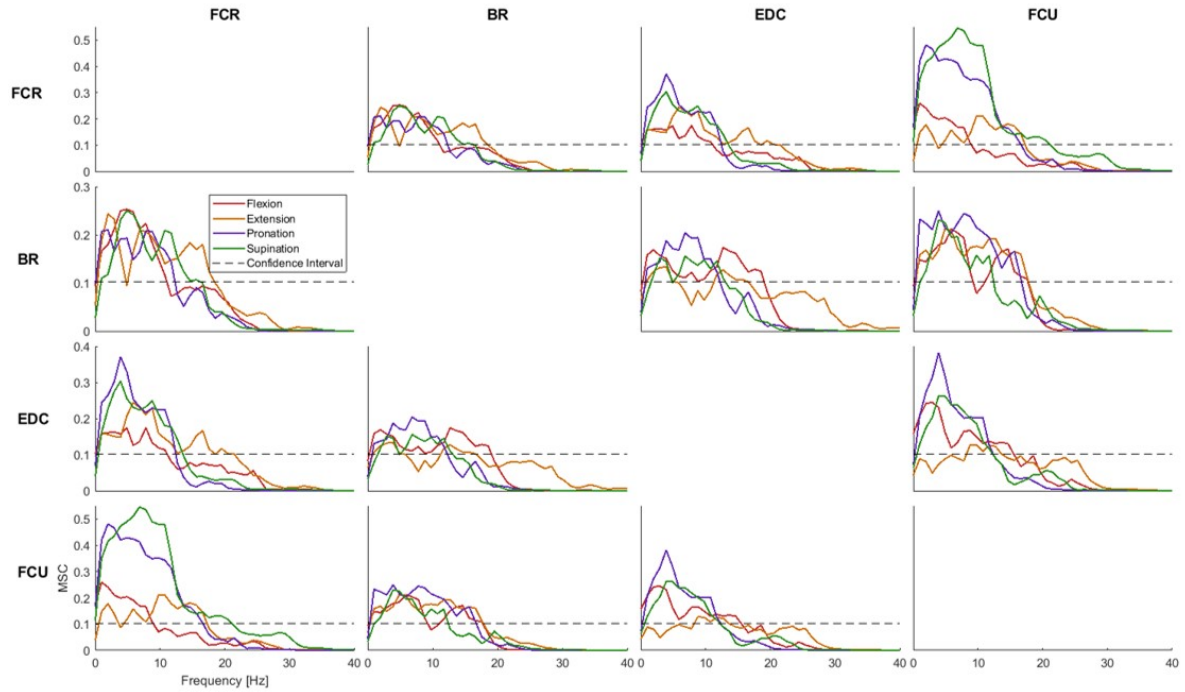

Fig. 3. Intermuscular coherence between all muscle pairs. Coherence is shown between all muscles (FCR, BR, EDC, and FCU) for all gestures (red: Flexion, yellow: Extension, purple: Pronation, and green: Supination).

all participants underwent a training trial which consisted of performing sustained contractions for two randomly selected gestures. Participants performed 5 repetitions of the first selected gesture, and similar to the existing literature in gesture detection [34] [35], and in motor unit activity decoding [36], intervals of 5 seconds of rest between each contraction were applied. After the last resting period, following the repetitions of the first gesture, participants performed 5 repetitions of the second gesture with similar resting intervals between each contraction. A 10-second interval was applied at the beginning and at the end of the trial. The training trial took 2 minutes per participant. Participants were asked to follow a digital clock presented on a monitor in front of them to keep track of the timing of each contraction. Fig 1 shows an illustration of the experimental layout. The experiment consisted of two groups of 2 randomly selected gestures. Similar to the training trial, performing each group of gestures lasted for 2 minutes. One minute of rest was applied between the two groups to prevent fatigue of the muscles. The order and grouping of the gestures were randomized. Both able-bodied and amputee groups followed the same experimental protocol. The experiment took 5 minutes per participant. Fig 1 shows an illustration of the cross-section view of the forearm and the positioning of the sensors. The non-symmetry of the sensor location illustrates the anatomical differences between participants. Muscles were palpated, and sensors were positioned over the target muscles. All amputee participants are quadruple amputees and needed to undergo amputation after sepsis. The first participant had the amputation 8 years ago and has a high-level trans-radial amputation on the tested limb. The participant makes regular use of a body-powered prosthesis on a day-to-day basis and maintains a high level of activity, including regular exercise and ADLs. The second and third amputee participants had the amputation 6 and 7 years ago, respectively, and have distal trans-radial amputations. Both participants use a Mitt prosthesis on average every 3-4 days for ADLs, maintaining a medium level of activity.

C. Data Processing

The raw acoustic signals of the MMG channels were analyzed to identify the onset and the offset of each contraction. In this study, and similar to the existing literature on gesture detection for electromyography [37], and mechanomyography [38], the signal was analyzed during the steady-state phase of the contraction in order to minimize the high degree of stochastic non-stationarity present in the transient phases. The transient state was discarded by removing the one-second post-onset and one-second pre-offset of the signal recorded for each contraction. The duration of the extracted signal was validated to ensure at least 3 seconds of a steady-state contraction.

In this work, MMG information was recorded using a sampling frequency of 1 kHz. The literature shows that the MMG power information resides in frequencies no higher than 120 Hz [17]. Numerous investigations have demonstrated that the dominant frequencies of muscle sound are found in the range of frequencies below 30 Hz [39] [40], and there is evidence showing MMG power information at frequencies as low as 2 Hz and as high as 118 Hz [41]. Thus, guided by the literature, the raw MMG signal was filtered using a fourth-order band-pass Butterworth filter in the range of 1 - 150 Hz.

Mechanomyography can be categorized as a signal with time-varying properties with power information at multiple frequencies. Therefore, a time-variant, frequency-selective ap-

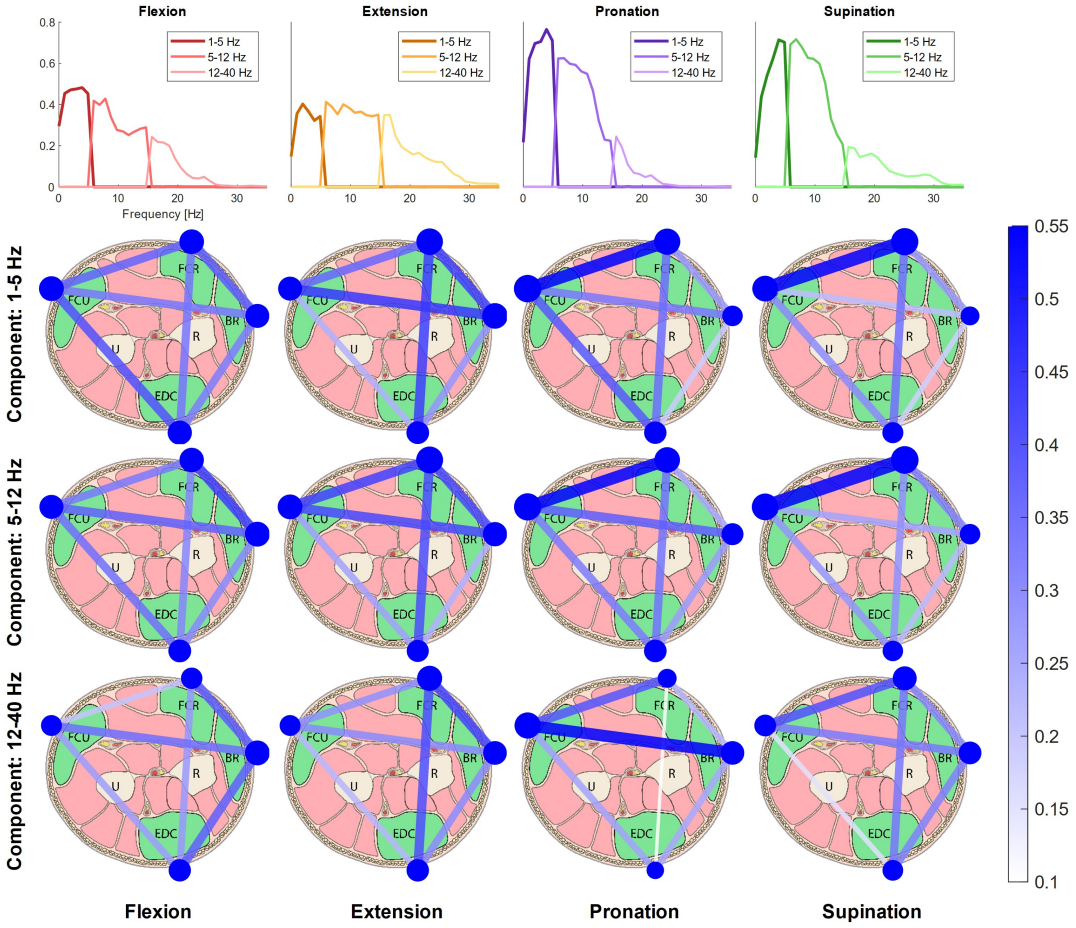

Fig. 4. The frequency content of the coherence spectra of all muscle combinations was averaged across subjects and decomposed into three components using non-negative matrix factorization. The three frequency components were defined as follows: component 1: 1-5 Hz, component 2: 5-12 Hz, component 3: 12-40 Hz. Top-row, common spectral patterns extracted for each gesture at every frequency component. Different shadings of color show the frequency ranges. Gestures are color-coded (red: Flexion, yellow: Extension, purple: Pronation, and green: Supination). Functional muscle networks were extracted for each gesture at each of the frequency components. Muscle networks were characterized by the extracted common frequency patterns and the weightings of those patterns in the original spectra. The weightings give the strength of the edges between the four muscles (nodes). The mapping of the color bar and the thickness of the edges show the strength of the connections between all muscle pairs. The size of the nodes denotes the degree of each connectivity for each muscle. Functional connectivity networks of all components (rows) are shown for each gesture (columns) for able-bodied participants.

proach is required for its analysis. A method widely investigated in the literature for time-frequency analysis is the Hilbert transform, a transform-based approach used for spectral analysis of time-varying signals which has shown to be equivalent to Fourier and wavelet analysis and from which coupling measures such as coherence can be derived [42]. In this way, the Hilbert transform was applied to the filtered MMG signal to obtain the analytic representation of the signal which was further used for the estimation of the cross-spectrum and the power spectral density, both necessary measures for the evaluation of intermuscular coherence.

D. Intermuscular Coherence

Intermuscular coherence is derived based on the magnitude square of the cross-spectrum between two signals normalized by the product of the power spectrum of the two signals (1). Because of the normalization, IMC is confined to be between the values 0 to 1. The closer the value of IMC to 1, the more linearly dependent (correlated) are the two signals in the frequency domain. A common problem in the estimation of coherence is the presence of spurious coherence due to spatial and spectral leakages [43]. In this study, in order to minimize the presence of spurious coherence caused by the filtering process and by the frequencies at which the spectral power information is critically close to zero, we implement a modified magnitude squared coherence (MMSC) method which includes a conditional statement based on the value of the product between the power spectrum of the two signals. The MMSC algorithm specifically avoids spurious coherence when the spectral information context of the signals has the least power. MMSC and IMC are used interchangeably for the rest of the paper. The mathematical derivation of MMSC can be found here:

$$MMSC_{xy} = \begin{cases} \frac{|S_{xy}|^2}{S_x * S_y}, & \text{if } S_x * S_y \geq 1 \\ \frac{|S_{xy}|^2}{1}, & \text{if } S_x * S_y < 1 \end{cases} \quad (1)$$

where,

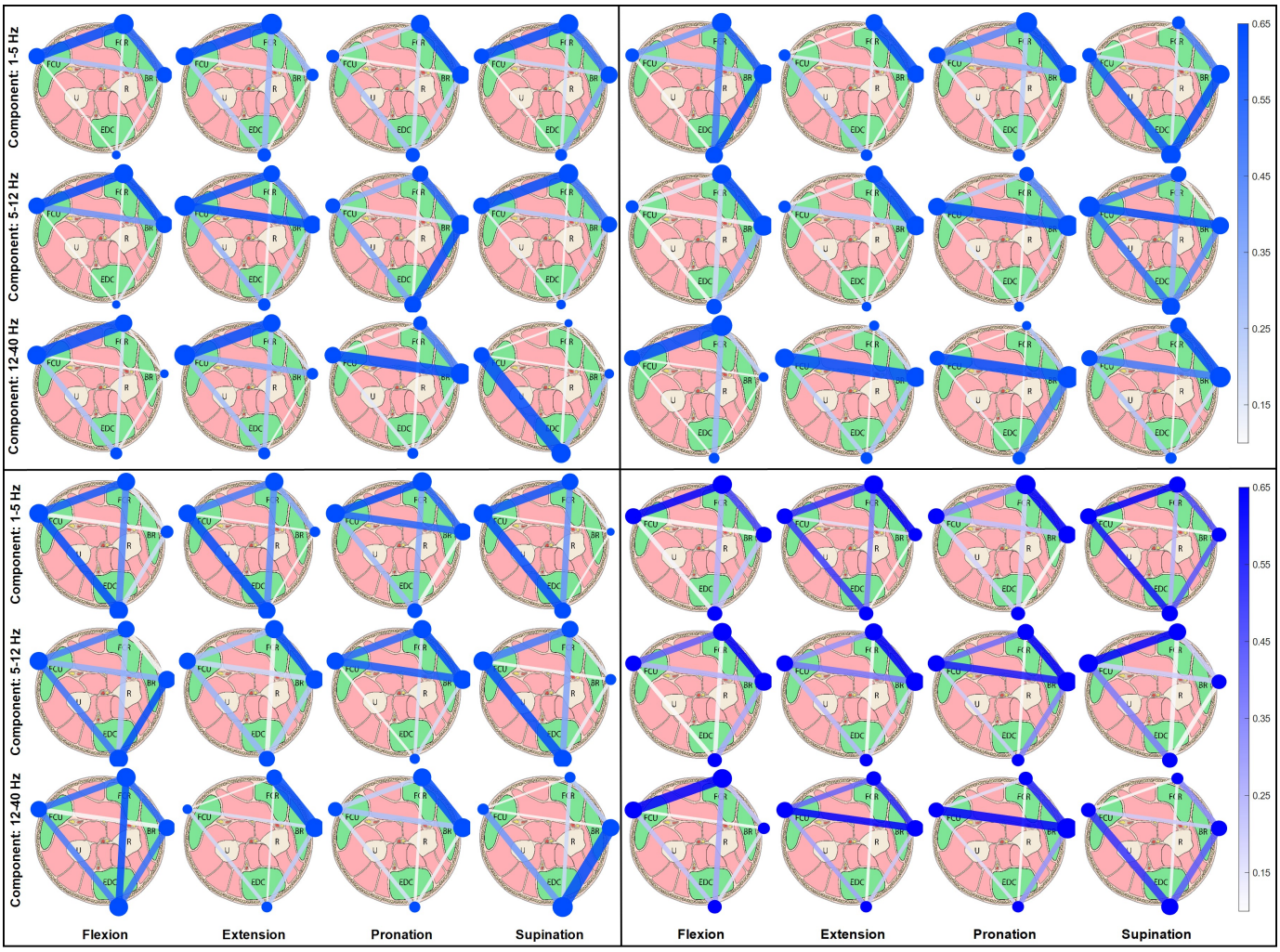

Fig. 5. The common spectral patterns of the coherence responses of all muscle combinations were decomposed into three components. Functional muscle networks were generated for each gesture at each of the frequency components. Muscle networks are generated from weightings of the common frequency patterns. The weightings give the strength of the edges between the four muscles (nodes). The thickness and color code of the edges shows the strength of the connections between muscles. The size of the node denotes the degree of connectivity of muscles. Functional connectivity networks are shown for all components (rows) for each gesture (columns) for all amputee participants (amputee 1: top-left, amputee 2: top-right, amputee 3: bottom-left, and average of amputees: bottom-right).

$MMSC_{xy}$ is the modified magnitude-squared coherence between signals x and y,
S_{xy} is the cross-spectrum between the signals,
S_x is the power spectral density of x, and
S_y is the power spectral density of y.

In this study, a method based on segment overlapping and tapering was applied in order to improve frequency resolution and reduce variance, as described in [44]. Coherence was evaluated using the following parameters: a segment of 1024 samples to obtain a frequency resolution of 0.98 Hz, a Nuttall window which helps reducing spectral leakage thanks to its significant side-lobe suppression, and 50% of overlap to account for the spectral resolution of the Nuttall window. To prevent non-stationarities and spurious coherence resulting from edge-effects caused from concatenation of trials, each 3-second trial of information was multiplied by a Tukey window using a cosine-tapered section of 0.05 [45]. Following this tapering process, the five trials of each gesture were concatenated to form a signal of 15 s duration. MMSC was calculated for all muscle pairs, gestures, and participants, resulting in a matrix of ($f_x m_x g_x s$), denoting f coherence values, m muscle pairs, g number of gestures, and s number of subjects.

E. Non-negative Matrix Factorization

A common method for deeper analysis of muscle networks is to decompose the full-spectrum coherence between different muscle groups into frequency-based connectivity using mathematical factorization methods (such as non-negative matrix factorization (NNMF), principal component analysis (PCA), or independent component analysis (ICA)). This allows identifying the common frequency space at which muscles are co-modulated by the neural drive. Non-negative matrix factorization is a multivariate method which is characteristic for its non-negative constraints [46]. NNMF has been widely used in the literature to identify the coactivation of groups of muscles that contribute to a particular task, also known

as muscle synergies [47]. In this respect, muscle synergies are extracted by applying NNMF to the EMG envelopes [48] [49]. NNMF has also been used to identify unique spectral patterns shared by groups of muscles from the estimated coherence between pairs of muscles [10] [12] [13]. However, NNMF has not been applied yet for the analysis of MMG activity; in particular, for the spectral decomposition of the signal. In this study, we use NNMF to decompose the MMG spectral space into frequency band components to study the spectral characteristics of the signal and to identify the common spectral patterns shared by the target muscles when performing different hand gestures.

It is established in the literature that mechanomyography includes three main processes: (i) the gross lateral movement of the muscles caused by the asynchronous activation of muscle fibers, (ii) lateral oscillations occurring at the resonant frequency of the muscles, and (iii) dimensional changes of the active muscle fibers as well as gross limb displacements [50] [33]. Dimensional changes of the muscle and gross limb displacement account for the lowest frequencies of the signal [51], tremor contributions reflecting the oscillations of the motor system have been reported over a broad frequency band, typically below 12 Hz [52] [53], and muscle inner vibrations account for the higher frequencies, falling in the range of 10-40 Hz due to intrinsic muscle fibers oscillations [54] [55]. As reported in the aforementioned studies, the components comprising the MMG signal have been found to occur at different frequency ranges, with some level of overlapping. In this study, frequency bands have been defined as 1-5 Hz for low-frequency information due to the bulk movement and dimensional changes of the muscles, 5–12 Hz for oscillations due to tremor produced during isometric contractions, and 12–40 Hz to capture the mechanical inner vibrations due to intrinsic muscle fibers oscillations. In this way, non-negative matrix factorization was applied, according to (2), to extract three components in order to determine the common spectral patterns in the delta band for component 1, theta and alpha bands for component 2, and beta and gamma bands for component 3.

Using NNMF, the original dataset regarded as an $f_x m$ matrix X, where each row contains f non-negative coherence values evaluated at each discrete frequency of the m muscle pairs, is factorized into two low-rank non-negative matrices: W, an $f_x k$ matrix with the activation patterns (common spectral patterns) of k components, and H, a $k_x m$ matrix denoting the weight coefficients (strength of muscle-pair connection) of each muscle pair for every component.

$$X \approx W.H \tag{2}$$

Non-negative matrix factorization was used to decompose the full-spectrum of the signal into frequency band components with their corresponding coupling strength across all muscle pairs for all gestures and subjects. In this way, NNMF was applied to each coherence matrix $f_x m$ (513 coherence values $_x$ 6 muscle pairs) corresponding to each gesture for all participants. In this paper, we use the multiplicative update rule for NNMF to minimize the objective function, as described in

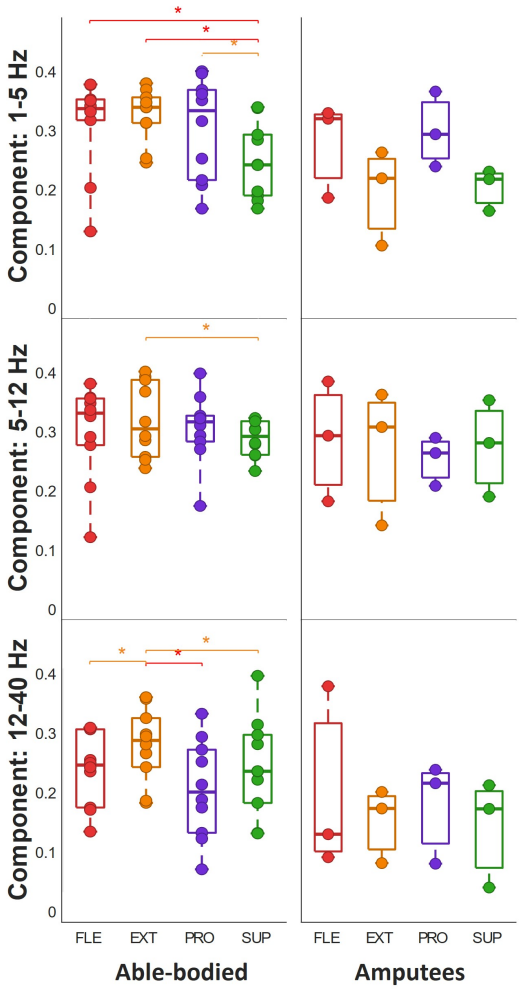

Fig. 6. Clustering coefficient (CC) was used to statistically compare the functional muscle networks across gestures (red: Flexion, yellow: Extension, purple: Pronation, and green: Supination) and frequency components (from top to bottom: 1-5 Hz, 5-12 Hz, and 12-40 Hz). The clustering coefficient was evaluated for each undirected weighted network for able-bodied (left column) and amputees (right column). A two-sample t-test was used to statistically compare the CC between gestures for able-bodied participants. Significance is shown in orange color for *p-value*$<$0.05, Bonferroni-adjusted significance is shown in red color for *adjusted-p-value*$<$0.0028

[56]. Different initialization methods for NNMF have been investigated in the literature to achieve a smaller error in the approximation and faster convergence [57] [58]. In this study, we introduce a similar initialization method to that proposed in [58]; however, instead of imposing a sparse structure in the spatial organization of the vectors, we constraint the scope of each component by initializing the columns of the W matrix. Each column of the W matrix representing a frequency band component (k_1: frequency band 1-5 Hz, k_2: frequency band 5-12 Hz, k_3: frequency band 12-40 Hz) was initialized with a uniform random amplitude distribution in the range [0.9, 1] only for their respective active frequency band. As expected, this initialization method resulted in delineated segregation of frequency bands for the common spectral patterns extracted (see Fig 4 top-row).

F. Connectivity Analysis

Coherence muscle networks were constructed after identifying the common spectral response of the muscle pairs at different frequencies by using NNMF. The spectral activation patterns represent the unique frequencies shared by the muscles during the hand gesture tasks. The weight coefficients produced from the factorization were used to construct the adjacency matrices. Task- and frequency-specific matrices were obtained, as NNMF extracted three components from the coherence spectra for each gesture and participant. These adjacency matrices were then used to construct the undirected weighted functional connectivity networks.

Clustering coefficient (CC) is a measure of functional segregation and is denoted by the extent to which neighbors of each node are connected to each other [59]. The mean of the clustering coefficient reflects the average of the clustered connectivity across nodes [60], with highly functional segregated networks indicated by higher values of averaged CC and vice versa. Based on the generalization of the algorithm to weighted undirected networks [61], the clustering coefficient was computed at all frequency bands for each of the connectivity networks for all gestures and participants. The average of CC across nodes was subsequently calculated to obtain a value of CC for each component, gesture, and participant.

G. Statistical Analysis

The clustering coefficient of the networks was compared between gestures for all participants to obtain statistical significance at each of the frequency band components. The data passed the Shapiro–Wilk normality test. Thus, a t-test was applied to determine significance of CC between gestures. CC at each frequency component was considered significantly different between gestures for $p\text{-}values < 0.05$. Bonferroni-adjusted significance level was calculated to account for the increased possibility of type-I error. The adjusted significance level is $adjusted\text{-}p\text{-}value = 0.0028$.

III. Results & Discussion

In this work, we analyzed muscle networks based on MMG activity recorded from four superficial muscles of the forearm while participants performed four different hand gestures. The power spectral density (PSD) was generated to analyze the spectral content of the MMG signal. PSD was averaged across homologous muscles, trials, and subjects. Fig 2 shows the different PSD profiles of all muscles across gestures for able-bodied and amputee participants. PSD for able-bodied participants shows a broad spectrum with peaks between 2-4 Hz and similar frequency profiles across muscles with differences in scaling depending on the gesture (Fig. 2). PSD for amputee participants reveals distinctively different profiles across muscles with peaks found between 2-12 Hz depending on the hand gesture. PSD profiles for amputees show a shift of peaks towards higher frequencies compared to the PSD generated able-bodied participants. PSD for both demographics showed power information at frequencies no higher than 40 Hz.

A. Coherence Matrix

Functional muscle networks were defined by mapping the correlated spectral response of different muscles for each gesture for able-bodied and amputee participants. The nodes of the networks represent the target muscles, and the edges of the networks represent the strength of functional connections between muscles. Fig 3 shows the intermuscular coherence between all muscle pairs of able-bodied subjects along with the confidence interval generated according to the method described in [44]. The common frequency components across all muscle pairs, hand gestures, and subjects for both demographics were extracted. Coherence for all muscle pairs were averaged across subjects to obtain coherence profiles for each gesture. The results show distinct functional organization for different hand gestures. Coherence is observed over a range of frequencies below 40 Hz, and distinctive frequency profiles were found depending on the muscle-pair and hand gesture. No values of coherence were found at frequencies higher than 40 Hz. The IMC results in Fig. 3 imply a dense connectivity matrix for all muscle pairs, showing high levels of common spectral patterns across different frequency bands. In the case of Flexion, different levels of IMC were found at frequencies below 12 Hz across all muscle pairs. The highest level of IMC for this gesture was found at 2 Hz for muscle pair FCR-FCU. Similar coherence profiles were found for Extension, with most of the IMC found at frequencies below 12 Hz and some level of IMC present at frequencies higher than 12 Hz for the muscle pairs BR-EDC and FCU-EDC. Pronation showed the highest levels of IMC for all the muscles connected to FCU, with peaks just below 5 Hz for muscle pairs FCU-EDC and FCU-BR and high IMC for all frequencies below 12 Hz for muscle pair FCU-FCR. A closely similar IMC profile was observed for Supination for FCU-FCR. Regarding the IMC pattern of FCU-FCR, it can be highlighted that two distinct behaviors are observed, one of which relates to similar patterns for Flexion and Extension (red and yellow lines), and the other one relates to a similar behavior comparing Pronation and Supination (purple and green lines).

B. Muscle Connectivity Networks

In order to evaluate the coherence over specific frequency ranges, intermuscular coherence was decomposed into three frequency bands using non-negative matrix factorization [46]. The number of components extracted evaluates the functional connection between muscles at low (1-5 Hz), medium (5-12 Hz), and high frequencies (12-40 Hz).

1) Able-bodied: The common spectral patterns for the three frequency components for each gesture were extracted using NNMF. The corresponding weightings for each component yield the functional connectivity matrices of the muscle networks for each gesture. Fig 4 shows the functional connectivity networks for able-bodied participants, generated for all gestures at each one of the frequency components.

The first component captures coherence at low frequencies and shows relatively high connectivity between all muscle pairs for Flexion and Extension. Pronation and Supination

TABLE I
STATISTICAL RESULTS OF CLUSTERING COEFFICIENTS

	comp.	Flexion	Extension	Pronation	Supination
Flexion	k1		t:-0.892 p:0.38	t:0.385 p:0.7	t:3.53 p:0.00068 Δ:-18.4% ↓
	k2		t:-1.11 p:0.27	t:-0.356 p:0.72	t:0.779 p:0.44
	k3		t:-2.51 p:0.014 Δ:16.7% ↑	t:1.78 p:0.079	t:-0.227 p:0.82
Extension	k1	t:-0.892 p:0.38		t:1.31 p:0.2	t:5.27 p:1.1e-06 Δ:-21.6% ↓
	k2	t:-1.11 p:0.27		t:0.869 p:0.39	t:2.34 p:0.022 Δ:-8.73% ↓
	k3	t:-2.51 p:0.014 Δ:-16.7% ↓		t:4.13 p:9.1e-05 Δ:-25.4% ↓	t:2.03 p:0.045 Δ:-12.5% ↓
Pronation	k1	t:0.385 p:0.7	t:1.31 p:0.2		t:3.01 p:0.0036 Δ:-16.6% ↓
	k2	t:-0.356 p:0.72	t:0.869 p:0.39		t:1.39 p:0.17
	k3	t:1.78 p:0.079	t:4.13 p:9.1e-05 Δ:25.4% ↑		t:-1.85 p:0.067
Supination	k1	t:3.53 p:0.00068 Δ:18.4% ↑	t:5.27 p:1.1e-06 Δ:21.6% ↑	t:3.01 p:0.0036 Δ:16.6% ↑	
	k2	t:0.779 p:0.44	t:2.34 p:0.022 Δ:8.73% ↑	t:1.39 p:0.17	
	k3	t:-0.227 p:0.82	t:2.03 p:0.045 Δ:12.5% ↑	t:-1.85 p:0.067	

Frequency band components are represented as, k1: component 1-5 Hz, k2: component 5-12 Hz, and k3: component 12-40 Hz.
Significance is shown in orange color for $p\text{-value}<0.05$, Bonferroni-adjusted significance is shown in red color for $adjusted\text{-}p\text{-}value<0.0028$, df=18.

appear to have a lower level of connectivity for muscle pairs EDC-BR and FCR-BR.

The second component shows a similar topology to that of the first component for all gestures. High connectivity between FCR-FCU is shown for both components for Pronation and Supination.

The third component shows a distinctly different functional organization of the networks compared to the first two spectral components. Flexion shows high connectivity for all vertices connected to the BR muscle. Weaker connectivity is shown for the muscle triplet FCR-FCU-EDC compared to the first two spectral components. In the case of Extension, muscle triplet FCR-BR-EDC maintained a high level of connectivity while FCR-FCU and FCU-BR show reduced connectivity. As opposed to Flexion and Extension, Pronation shows an evidently strong connectivity for all muscles pairs connected to FCU. connectivity between FCR-BR and EDC-BR show similar connectivity to that shown in the other two spectral components. Lastly, Supination shows a distinct topology related to the third spectral component, showing lower connectivity between the muscle pair FCR-FCU and FCU-EDC but higher connectivity between the rest of the muscle pairs. FCR-BR shows a similar level of connectivity compared to the first two spectral components. Muscle networks in Fig 4 indicate a gradual transition from widespread connectivity between all muscle pairs for the lowest frequency component to strong localized connections for the third frequency band. This analysis also suggests a distinct signature of MMG-based connectivity for different gestures.

2) Amputees: Fig 5 illustrates the functional connectivity networks for each amputee participant and the mean of the participants for all gestures at each frequency component.

For each amputee participant, the first component shows high connectivity between muscle pair FCR-FCU for Flexion, medium to high levels of connectivity between FCR-BR for Extension, and low levels of connectivity for both gestures between FCU-BR. Pronation shows high connectivity between FCR-BR, medium levels of connectivity between EDC-FCR, and medium to low connectivity between FCU-EDC and EDC-BR. Supination shows low connectivity between FCU-BR and heterogeneous connectivity for the rest of the muscle pairs across participants.

The second component shows widespread connectivity between all muscle pairs for Flexion and Extension for two of the amputee participants, and a strong connection between FCR-BR for Flexion, Extension and Pronation for all participants. Strong connections were also found for all vertices connected to BR for Pronation, with low connectivity between EDC-BR. Interestingly, a similar topology to that of the first component was shown for Supination across all participants.

The third component shows a decrease in connectivity in muscle pair BR-FCU and high connectivity between FCR-FCU for Flexion for all participants. Heterogeneous connectivity between all muscle pairs across participants was found for Extension with medium levels of connectivity between EDC-BR and FCU-EDC and low connectivity for FCR-EDC. A similar topology was found for Pronation with higher connectivity between FCU-BR. For Supination, all participants showed high and medium levels of connectivity for FCU-EDC and EDC-BR, respectively, while medium to low connectivity was found for the rest of the muscle pairs.

3) Able-bodied vs Amputees: The first component shows a similar network topology to that of the second component across all gestures for able-bodied and for each of the amputee participants. The third component shows different topologies and lower connectivity compared to the first two components for both demographics. These results suggest overlapping frequency information for the bulk movement of the muscles and the tremor produced during the contractions. The distinct topologies at higher frequencies suggest that muscle fibers oscillations produce localized spectral activity for specific muscle pairs depending on the gesture.

It is important to mention that opposite gestures reflect a similar topology of connectivity for the first two frequency components for all amputee participants and, more evidently, for able-bodied participants. In other words, Flexion and Extension show a similar connectivity topology, and Pronation and Supination present the same phenomena. This could be a result of the fact that MMG captures not only the contraction of the agonist muscles but also the relaxation of the antagonist muscles, both simultaneously occurring during the task and found to be present at low frequencies [62]. Interestingly, similar topologies were found between Extension and Pronation across all frequency components for each amputee participant.

The third component showed a different topology between able-bodied and amputees for all gestures, with some similarity in connectivity strength for BR muscle pairs for Extension and Pronation

Regarding the role of each muscle during the gestures, all four muscles are involved when performing wrist Flexion and Extension. Able-bodied participants showed widespread connectivity between muscles for the first two components with some localized connectivity in the FCR and BR muscles for the third component. Similarly, high connectivity was found for FCR and BR muscles for two of the amputee participants across the same gestures in the first two components, with also high connectivity present in the FCU muscle for both participants. In general, for each amputee participant, EDC appeared to be the least active muscle for Flexion and Extension for the first two components.

The brachioradialis muscle is responsible for bringing the pronated, or supinated forearm into a neutral position. Thus, in the case of Pronation and Supination, it is expected to find a higher level of connectivity for vertices connected to BR due to its role in both actions. Interestingly, similar topologies were found between Extension and Pronation across all frequency components for each amputee participant. The third component showed a different topology between able-bodied and amputees for all gestures, with some similarity in connectivity strength for some muscle pairs for Extension and Pronation.

A low level of connectivity is expected for the EDC muscle during Pronation and Supination due to the role that the EDC muscle has during these gestures. The extensor digitorum communis muscle is a multi-compartment muscle that is responsible for extending digits 2–5. Given that extension of the fingers occurred only during Flexion and Extension, the connectivity of the muscle is expected to be higher for these gestures than for Pronation and Supination. This is evident for able-bodied participants, particularly for the third frequency component. However, this is not the case for amputee participants, where a low level of connectivity is found for the EDC muscle compared to the rest of the muscles across all frequency components for all gestures. These differences in muscle pair connectivity strengths, and therefore on the topology of the networks between demographics might be present because of the anatomical differences caused by amputation, variations of remaining muscle, and level of muscle activity. These functional (re)organization differences between able-bodied and amputees could show not only how the anatomy has changed after amputation but also how the neural drive adapts to those anatomical changes when performing the same gestures. To better investigate this phenomenon, our future line of research includes participating more amputees to provide stronger statistics regarding the observed changes reported here.

C. Network Analysis

Complex network analysis was used to compare the muscle networks between hand gestures for the different frequency components. In order to analyze network segregation, the clustering coefficient (CC) was derived from all networks. In this work, a t-test was used to evaluate the statistical significance of the network behaviors. Fig 6 shows the results of the t-test for the CC of all the undirected networks. Significant differences between gestures are shown in orange for ($p < 0.05$) and in red after applying Bonferroni correction for ($p < 0.0028$). For able-bodied participants, the first frequency component showed that CC for Flexion and Extension were significantly higher than CC for Supination ($p < 0.0028$). CC for Pronation was also found to be significantly higher than CC for Supination ($p < 0.05$). The second frequency component shows a significant difference in CC between Extension and Supination only ($p < 0.05$). On average, similar values of CC were found between the rest of the gestures. Similar to the first component, Supination showed the lowest values of CC across all gestures. The third frequency component shows that CC for Extension is significantly higher than CC for Flexion, and CC for Supination is significantly higher than CC for Extension ($p < 0.05$). Pronation showed a significantly lower value of CC compared to Extension ($p < 0.0028$). Table I summarizes the statistical results of the clustering coefficient for all frequency bands and gestures for able-bodied participants. For amputee participants, the first component showed distinct distributions of CC values for all gestures. The individual contributions of each amputee participant can be seen in Fig 6. Similar to able-bodied participants, the second frequency component showed the least variability of CC between gestures compared to the other frequency components. The third frequency component showed a distinctively wider distribution for Flexion compared to the other gestures which showed similar distributions of CC.

In this study, we have shown distinct muscle connectivity topologies depending on the frequency component, gesture, and demographic. Significant differences in functionally segregated networks for specific gestures at low and high frequencies were found. The differences of CC between Supination and the rest of the muscles for the first frequency component for able-bodied participants suggest a characteristic spectral profile for the muscle displacement that occurs during Supination. The differences of CC between Extension and the rest of the muscles for the third component suggest common spectral characteristics between muscles at higher frequencies for this particular gesture compared to the other gestures. The above-mentioned analysis and the results given in Table I show a clear distinction of functional muscle networks registered using MMG and calculated by intermuscular coherence at different frequency bands. The results also highlight potential differences in the MMG frequency spectra between able-bodied and amputees. This work, for the first time, provides a strong biomarker of synergistic muscle functionality using the clustering coefficient of the network extracted using MMG activity. Different types of time and frequency analysis methods have been suggested to analyze the MMG signal features and its role in motor control [17], [63]. MMG power spectrum has been reported to contain information regarding firing rate of motor units, with increases in the global firing rate of motor units resulting in higher frequencies of the MMG signal [64]. The results of the present study regarding differences in muscle connectivity networks across frequency components and clustering coefficient distributions may support the application of

MMG signal parameters as indicators of motor unit activation patterns and firing rates during muscle activity. The outcome of the study can further be used for the conduction of classifiers to find the motor intention of the user based on functional connectivity, with potential for real-time implementation of the MMG-based approach [65]. The results can also be used to track the changes in functional synergistic behavior of healthy and impaired muscles.

The present results show evidence that mechanomyography can be used as a tool to perform analysis of functional muscle networks for able-bodied and amputee users. However, this study presents several limitations. Miniaturization of the device is needed to make it a wearable system to be able to utilize the proposed novel MMG-based muscle network analysis in the control of prostheses. This study also did not consider complex dynamic activities which have shown to provide relevant information regarding muscle function [17]. So far, muscle network analysis has been done only by the use of EMG. This study did not include the simultaneous acquisition of EMG activity for the comparison of muscle networks obtained using each type of myographic signal. Previous research indicates that the motor unit recruitment and firing rate affect the MMG and EMG equally for contractions up to 80% MVC [54]. Therefore, it is to expect that muscle networks derived from both of these myographic modalities will reflect similarities in their topologies for low and medium levels of contraction. Future perspectives of this work will focus on (a) miniaturization of the device for translation of the proposed system into wearable technology to be used in a clinical setting, (b) evaluation of static and dynamic tasks for a deeper analysis of the neural circuitry involved in different types of motor tasks, and (c) simultaneous acquisition of electromyography and mechanomyography activity during different gestures for analysis and comparison of muscle networks derived from each myographic modality.

IV. Conclusion

In this study we present, for the first time, the analysis of functional muscle networks using MMG and mapping of its variance between able-bodied and amputee participants. Intermuscular coherence was derived from the frequency response of all the muscle pairs for all gestures and participants. Coherence was decomposed into three frequency components using non-negative matrix factorization. Muscle networks were generated for all gestures and all spectral components. Complex network analysis was conducted to extract the clustering coefficient of each network, which was used for statistical comparisons between gestures for able-bodied participants. Results showed significant differences between gestures across multiple frequency bands for able-bodied participants. These findings support the hypothesis that mechanomyography can be used for muscle network analysis and that it can be further exploited for the analysis of functional muscle connectivity for able-bodied and amputees. The findings of this investigation offer the concomitant outcomes of supporting the usability of MMG to map muscle coherence from a neurophysiological perspective as well as providing a mechanistic basis for its translation into human-robot interfaces (e.g., prosthetic hand control). It is important to mention that further analysis including the simultaneous acquisition of MMG and EMG activity is expected as the next step of this research in order to analyze muscle networks derived from each myographic signal and study the contributions of each modality in the analysis of functional muscle connectivity. In addition, the results of the present study motivate the investigation of a wider range of research questions, including MMG spectral analysis of a wider range of activities requiring different sets of muscles in the upper and lower limbs. Translation is underway with corporate collaborators (https://sergtechnologies.com/) in artificial limbs and tremor control.

References

[1] E. Bizzi and V. C. Cheung. The neural origin of muscle synergies. *Frontiers in Computational Neuroscience*, 7:51, 2013.

[2] A. d'Avella and E. Bizzi. Shared and specific muscle synergies in natural motor behaviors. *Proceedings of the National Academy of Sciences of the United States of America*, 102(8):3076–3081, Feb 2005.

[3] C. B. Hart and S. F. Giszter. A neural basis for motor primitives in the spinal cord. *The Journal of neuroscience : the official journal of the Society for Neuroscience*, 30(4):1322–1336, Jan 2010.

[4] L. H. Ting et al. Neuromechanical principles underlying movement modularity and their implications for rehabilitation. *Neuron*, 86(1):38–54, 2015.

[5] T. W. Boonstra and M. Breakspear. Neural mechanisms of intermuscular coherence: implications for the rectification of surface electromyography. *Journal of Neurophysiology*, 107(3):796–807, 2012. PMID: 22072508.

[6] J. I. Chapeton et al. Large-scale communication in the human brain is rhythmically modulated through alpha coherence. *Current Biology*, 29(17):2801–2811.e5, 2019.

[7] X. Xi et al. Enhanced eeg–emg coherence analysis based on hand movements. *Biomedical Signal Processing and Control*, 56:101727, 2020.

[8] J. M. Kilner et al. Human cortical muscle coherence is directly related to specific motor parameters. *The Journal of neuroscience : the official journal of the Society for Neuroscience*, 20(23):8838–8845, Dec 2000.

[9] Y. Gao et al. Electroencephalogram-electromyography coupling analysis in stroke based on symbolic transfer entropy. *Frontiers in neurology*, 8:716–716, Jan 2018.

[10] T. W. Boonstra et al. Muscle networks: Connectivity analysis of EMG activity during postural control. *Scientific Reports*, 5(1), dec 2015.

[11] J. N. Kerkman et al. Functional connectivity analysis of multiplex muscle network across frequencies. In N. Lovell, editor, *2017 39th Annual International Conference of the IEEE Engineering in Medicine and Biology Society (EMBC 2017)*, Proceedings of the Annual International Conference of the IEEE Engineering in Medicine and Biology Society, EMBS, pp. 1567–1570, United States of America, sep 2017. IEEE, Institute of Electrical and Electronics Engineers. International Conference of the IEEE Engineering in Medicine and Biology Society 2017, EMBC 2017 Conference date: 11-07-2017 Through 15-07-2017.

[12] J. N. Kerkman et al. Network structure of the human musculoskeletal system shapes neural interactions on multiple time scales. *Science Advances*, 4(6), 2018.

[13] J. N. Kerkman et al. Muscle synergies and coherence networks reflect different modes of coordination during walking. *Frontiers in Physiology*, 11:751, 2020.

[14] C. M. Laine and F. J. Valero-Cuevas. Intermuscular coherence reflects functional coordination. *Journal of neurophysiology*, 118(3):1775–1783, Sep 2017.

[15] Y. Lin et al. Muscle connectivity analysis for hand gesture recognition via semg. In *2018 Asia-Pacific Signal and Information Processing Association Annual Summit and Conference (APSIPA ASC)*, pp. 848–852, 2018.

[16] M. Houston et al. Alterations in muscle networks in the upper extremity of chronic stroke survivors. *IEEE Transactions on Neural Systems and Rehabilitation Engineering*, pp. 1–1, 2021.

[17] M. O. Ibitoye et al. Mechanomyography and muscle function assessment: A review of current state and prospects. *Clinical Biomechanics*, 29(6):691–704, 2014.

[18] C. Orizio et al. The surface mechanomyogram as a tool to describe the influence of fatigue on biceps brachii motor unit activation strategy. historical basis and novel evidence. *European Journal of Applied Physiology*, 90(3):326–336, Oct 2003.

[19] T. W. Beck et al. Mechanomyographic and electromyographic time and frequency domain responses during submaximal to maximal isokinetic muscle actions of the biceps brachii. *European Journal of Applied Physiology*, 92(3):352–359, Jul 2004.

[20] C. Orizio et al. Surface mechanomyogram reflects muscle fibres twitches summation. *Journal of Biomechanics*, 29(4):475–481, 1996.

[21] R. Uwamahoro et al. Assessment of muscle activity using electrical stimulation and mechanomyography: a systematic review. *BioMedical Engineering OnLine*, 20(1):1, Jan 2021.

[22] R. B. Woodward et al. Segmenting mechanomyography measures of muscle activity phases using inertial data. *Scientific Reports*, 9(1):5569, Apr 2019.

[23] M. J. Stokes and P. A. Dalton. Acoustic myography for investigating human skeletal muscle fatigue. *Journal of Applied Physiology*, 71(4):1422–1426, 1991. PMID: 1757365.

[24] J. T. Cramer et al. The relationships among peak torque, mean power output, mechanomyography, and electromyography in men and women during maximal, eccentric isokinetic muscle actions. *European Journal of Applied Physiology*, 86(3):226–232, Jan 2002.

[25] R. B. Woodward et al. Pervasive monitoring of motion and muscle activation: Inertial and mechanomyography fusion. *IEEE/ASME Transactions on Mechatronics*, 22(5):2022–2033, 2017.

[26] S. O. H. Madgwick et al. An extended complementary filter for full-body marg orientation estimation. *IEEE/ASME Transactions on Mechatronics*, 25(4):2054–2064, 2020.

[27] E. D. Ryan et al. Time and frequency domain responses of the mechanomyogram and electromyogram during isometric ramp contractions: A comparison of the short-time fourier and continuous wavelet transforms. *Journal of Electromyography and Kinesiology*, 18(1):54–67, 2008.

[28] T. W. Beck et al. Does the frequency content of the surface mechanomyographic signal reflect motor unit firing rates? a brief review. *Journal of Electromyography and Kinesiology*, 17(1):1–13, 2007.

[29] S. Wilson et al. Formulation of a new gradient descent marg orientation algorithm: Case study on robot teleoperation. *Mechanical Systems and Signal Processing*, 130:183–200, 2019.

[30] W. Guo et al. Mechanomyography assisted myoeletric sensing for upper-extremity prostheses: A hybrid approach. *IEEE Sensors Journal*, 17(10):3100–3108, 2017.

[31] C. S. M. Castillo et al. Wearable mmg-plus-one armband: Evaluation of normal force on mechanomyography (mmg) to enhance human-machine interfacing. *IEEE Transactions on Neural Systems and Rehabilitation Engineering*, 29:196–205, 2021.

[32] M. A. Islam et al. Longitudinal, lateral and transverse axes of forearm muscles influence the crosstalk in the mechanomyographic signals during isometric wrist postures. *PLOS ONE*, 9:1–8, 08 2014.

[33] M. A. Islam et al. Cross-talk in mechanomyographic signals from the forearm muscles during sub-maximal to maximal isometric grip force. *PLOS ONE*, 9:1–9, 05 2014.

[34] Y. Rajamani et al. Analysis and classification of multiple hand gestures using mmg signals. *Journal of Telecommunication, Electronic and Computer Engineering (JTEC)*, 10(1-13):67–71, May 2018.

[35] P. Kaczmarek et al. Towards sensor position-invariant hand gesture recognition using a mechanomyographic interface. In *2017 Signal Processing: Algorithms, Architectures, Arrangements, and Applications (SPA)*, pp. 53–58, 2017.

[36] T. Kapelner et al. Decoding motor unit activity from forearm muscles: Perspectives for myoelectric control. *IEEE Transactions on Neural Systems and Rehabilitation Engineering*, 26(1):244–251, 2018.

[37] F. Tenore et al. Decoding of individuated finger movements using surface electromyography. *IEEE transactions on bio-medical engineering*, 56:1427–34, 06 2009.

[38] N. Alves and T. Chau. Stationarity distributions of mechanomyogram signals from isometric contractions of extrinsic hand muscles during functional grasping. *Journal of Electromyography and Kinesiology*, 18(3):509–515, 2008.

[39] C. Orizio et al. Spectral analysis of muscular sound during isometric contraction of biceps brachii. *Journal of Applied Physiology*, 68(2):508–512, 1990. PMID: 2318762.

[40] C. Orizio. Muscle sound: bases for the introduction of a mechanomyographic signal in muscle studies. *Critical reviews in biomedical engineering*, 21(3):201—243, 1993.

[41] T. W. Beck et al. Time/frequency events of surface mechanomyographic signals resolved by nonlinearly scaled wavelets. *Biomedical Signal Processing and Control*, 3(3):255–266, 2008.

[42] A. Bruns. Fourier-, hilbert- and wavelet-based signal analysis: are they really different approaches? *Journal of Neuroscience Methods*, 137(2):321–332, 2004.

[43] K. Sekihara et al. Removal of spurious coherence in meg source-space coherence analysis. *IEEE Transactions on Biomedical Engineering*, 58(11):3121–3129, 2011.

[44] K. Terry and L. Griffin. How computational technique and spike train properties affect coherence detection. *Journal of Neuroscience Methods*, 168(1):212–223, 2008.

[45] P. Bloomfield. *Fourier analysis of time series: An introduction*. Wiley-Interscience, New York, 2000.

[46] D. D. Lee and H. S. Seung. Learning the parts of objects by non-negative matrix factorization. *Nature*, 401(6755):788–791, Oct 1999.

[47] W. Lee. Neuromotor synergies as a basis for coordinated intentional action. *Journal of motor behavior*, 16(2):135—170, June 1984.

[48] L. Pellegrino et al. Evaluating upper limb impairments in multiple sclerosis by exposure to different mechanical environments. *Scientific Reports*, 8(1):2110, Feb 2018.

[49] M. Rabbi et al. Non-negative matrix factorisation is the most appropriate method for extraction of muscle synergies in walking and running. *Scientific Reports*, 10, 05 2020.

[50] M. H. Malek and J. W. Coburn. The utility of electromyography and mechanomyography for assessing neuromuscular function: A noninvasive approach. *Physical Medicine and Rehabilitation Clinics of North America*, 23(1):23–32, 2012. Recent Advancements in Neuromuscular Medicine.

[51] A. S. Wee and R. A. Ashley. Vibrations and sounds produced during sustained voluntary muscle contraction. *Electromyography and clinical neurophysiology*, 29 6:333–7, 1989.

[52] J. H. McAuley et al. Frequency peaks of tremor, muscle vibration and electromyographic activity at 10 hz, 20 hz and 40 hz during human finger muscle contraction may reflect rhythmicities of central neural firing. *Experimental Brain Research*, 114(3):525–541, May 1997.

[53] T.-K. Kim et al. Comparison of an accelerometer and a condenser microphone for mechanomyographic signals during measurement of agonist and antagonist muscles in sustained isometric muscle contractions. *Journal of PHYSIOLOGICAL ANTHROPOLOGY*, 27(3):121–131, 2008.

[54] C. Orizio et al. Muscular sound and force relationship during isometric contraction in man. *European Journal of Applied Physiology and Occupational Physiology*, 58(5):528–533, 1989.

[55] D. Barry. Vibrations and sounds from evoked muscle twitches. *Electromyography and clinical neurophysiology*, 32(1-2):35—40, 1992.

[56] M. W. Berry et al. Algorithms and applications for approximate nonnegative matrix factorization. *Computational Statistics & Data Analysis*, 52(1):155–173, 2007.

[57] Z. Zheng et al. Initialization enhancer for non-negative matrix factorization. *Engineering Applications of Artificial Intelligence*, 20(1):101–110, 2007.

[58] M. H. Soomro et al. Comparison of initialization techniques for the accurate extraction of muscle synergies from myoelectric signals via nonnegative matrix factorization. *Applied Bionics and Biomechanics*, 2018:3629347, May 2018.

[59] D. J. Watts and S. H. Strogatz. Collective dynamics of 'small-world' networks. *Nature*, 393(6684):440–442, Jun 1998.

[60] M. Rubinov and O. Sporns. Complex network measures of brain connectivity: Uses and interpretations. *NeuroImage*, 52(3):1059–1069, 2010. Computational Models of the Brain.

[61] J.-P. Onnela et al. Intensity and coherence of motifs in weighted complex networks. *Phys. Rev. E*, 71:065103, Jun 2005.

[62] T.-K. Kim et al. Influence of force tremor on mechanomyographic signals recorded with an accelerometer and a condenser microphone during measurement of agonist and antagonist muscles in voluntary submaximal isometric contractions. *Journal of PHYSIOLOGICAL ANTHROPOLOGY*, 27(1):33–42, 2008.

[63] E. Cé et al. Novel insights into skeletal muscle function by mechanomyography: from the laboratory to the field. *Sport Sciences for Health*, 11:1–28, 2015.

[64] K. Akataki et al. Mechanomyographic responses during voluntary ramp contractions of the human first dorsal interosseous muscle. *European Journal of Applied Physiology*, 89:520–525, 2003.

[65] N. Alves and T. Chau. Automatic detection of muscle activity from mechanomyogram signals: a comparison of amplitude and wavelet-based methods. *Physiological Measurement*, 31(4):461–476, feb 2010.